RESEARCH ARTICLE

National Science Review
12: nwaf220, 2025
https://doi.org/10.1093/nsr/nwaf220
Advance access publication 29 May 2025

PHYSICS

Special Topic: Uncovering the Mechanism of Nickelate Superconductors

Identification of superconductivity in bilayer nickelate $La_3Ni_2O_7$ under high pressure up to 100 GPa

Jingyuan Li[1,†], Di Peng[2,†], Peiyue Ma[1], Hengyuan Zhang[1], Zhenfang Xing[3], Xing Huang[1], Chaoxin Huang[1], Mengwu Huo[1], Deyuan Hu[1], Zixian Dong[1], Xiang Chen[1], Tao Xie[1], Hongliang Dong[2,3], Hualei Sun[4,*], Qiaoshi Zeng[2,3,*], Ho-kwang Mao[2,3] and Meng Wang[1,*]

[1]Center for Neutron Science and Technology, Guangdong Provincial Key Laboratory of Magnetoelectric Physics and Devices, School of Physics, Sun Yat-Sen University, Guangzhou 510275, China; [2]Shanghai Key Laboratory of Material Frontiers Research in Extreme Environments (MFree), Institute for Shanghai Advanced Research in Physical Sciences (SHARPS), Shanghai 201203, China; [3]Center for High Pressure Science & Technology Advanced Research, Shanghai 201203, China and [4]School of Science, Sun Yat-Sen University, Shenzhen 518107, China

***Corresponding authors.** E-mails: sunhlei@mail.sysu.edu.cn; zengqs@hpstar.ac.cn; wangmeng5@mail.sysu.edu.cn

†Equally contributed to this work.

Received 6 May 2025; **Accepted** 20 May 2025

ABSTRACT

Identification of superconductivity in the Ruddlesden-Popper phases of nickelates under high pressure remains challenging. Here, we report a comprehensive study of the crystal structure, electrical resistance, and Meissner effect in single crystals of bilayer nickelate $La_3Ni_2O_7$ under hydrostatic pressures up to 104 GPa. Using high-pressure X-ray diffraction, we observe a structural transition from an orthorhombic to a tetragonal phase above 40 GPa. Superconductivity emerges with a maximum onset transition temperature T_c^{onset} of 83 K at 18.0 GPa, accompanied by zero resistance. The superconducting phase is gradually suppressed and vanishes above 80 GPa, forming a right-triangle-like superconducting region. Direct-current magnetic susceptibility measurements demonstrate the Meissner effect and reveal a superconducting volume fraction of ∼41% at 22.0 GPa and 20 K, confirming the bulk nature of superconductivity in $La_3Ni_2O_7$. Our results highlight the intricate relationship between superconductivity, oxygen content, and structural transitions in this material.

Keywords: nickelates, high-temperature superconductivity, Ruddlesden-Popper phase, high-pressure technique, Meissner effect

INTRODUCTION

The discovery of high-temperature superconductivity in cuprates has spurred extensive research into nickelates, which share similar lattice and electronic structures. In particular, the Ni^+ ion in $ReNiO_2$ (Re = La, Nd, Sm, etc.) exhibits a spin configuration analogous to Cu^{2+} in cuprates [1,2]. However, superconductivity in nickelates remained elusive until the discovery of a superconducting (SC) transition at T_c = 15 K in $Nd_{0.8}Sr_{0.2}NiO_2$ thin films in 2019 [3–5]. Ni ions with a valence state close to Ni^+ and a spin S = 1/2 in planar coordination with oxygen ions were thought to be crucial for the emergence of superconductivity in nickelates [2,6].

The recent observation of superconductivity in the Ruddlesden-Popper (RP) phase nickelate $La_3Ni_2O_7$ with $T_c \sim 80$ K has reignited interest in this field [7–12]. The SC phase in $La_3Ni_2O_7$ is characterized by a bilayer structure with a '2222' stacking sequence of NiO_6 octahedra, which undergoes a structural transition from an orthorhombic *Amam* phase to a high-pressure orthorhombic *Fmmm* phase at 14.0 GPa [7]. This transition is accompanied by a change in the Ni-O-Ni bond angle along the *c*-axis from 168° to 180°. Scanning transmission electron microscopy (STEM) [13] and X-ray diffraction (XRD) studies [14] have confirmed the '2222' stacking sequence in single crystals of $La_3Ni_2O_7$ grown by the high-pressure floating zone method and polycrystalline samples of $La_3Ni_2O_7$ [15] and $La_2PrNi_2O_7$ [16] grown by the sol-gel method. Oxygen vacancies, particularly at the inner apical oxygen site shared by two NiO_6 octahedra, have been visualized using STEM [13]. Further structural

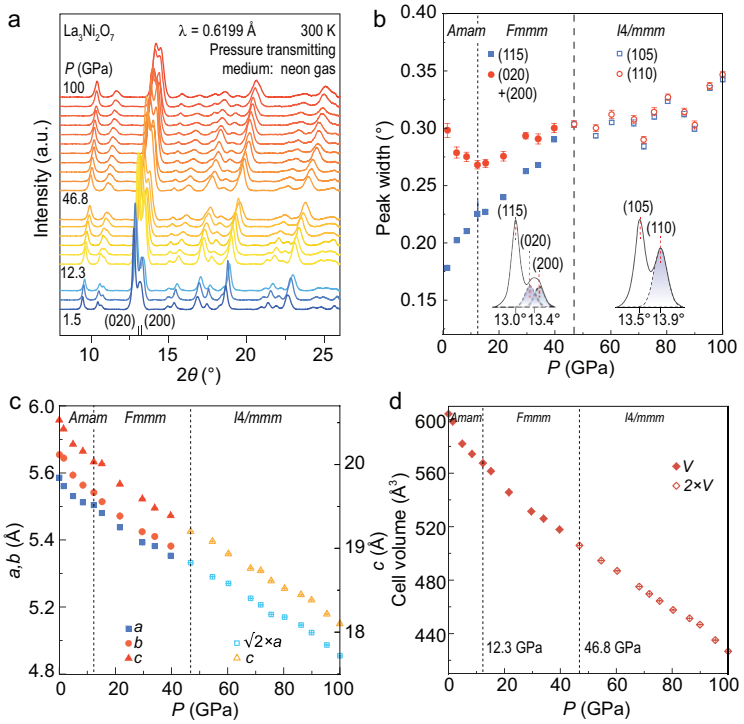

Figure 1. High-pressure structural characterizations of $La_3Ni_2O_7$ up to 100 GPa. (a) Synchrotron XRD patterns of $La_3Ni_2O_7$ under pressures from 1.5 to 100 GPa. The pressure transmitting medium (PTM) is neon gas. (b) Pressure dependence of the peak widths of (020)/(200) as a whole and (115) in the *Amam* space group. A merging of the peak widths at 12.3 GPa signals a structural transition from the *Amam* phase to the *Fmmm* phase. The peak widths of (020)/(200) become indistinguishable from those of (115) above 46.8 GPa, indicating a structural transition from *Fmmm* to tetragonal *I4/mmm* space group. The reflection indexes of (115) and (020)/(200) in the *Amam* space group change to (105) and (110) in the *I4/mmm* space group. The insets are the zoom-in experimental data. (c) Lattice parameters of $La_3Ni_2O_7$ obtained from the synchrotron XRD data. (d) Cell volumes of $La_3Ni_2O_7$.

analysis under high pressure and low temperature has revealed a tetragonal *I4/mmm* phase associated with the SC state [17]. In addition, a new structure of $La_3Ni_2O_7$ with an alternating monolayer-trilayer NiO_6 octahedra stacking sequence, denoted as the '1313' phase, was identified [18–21]. The properties of the distinct structure under high pressure remain unclear.

Despite these advances, several questions remain unresolved. For instance, the difficulty in achieving zero resistance and the weak suppression of T_c in $La_3Ni_2O_7$ under pressures below 43.5 GPa have raised concerns about the nature of superconductivity in this material [7,9–11]. Additionally, the low SC volume fraction observed in alternating-current (AC) magnetic susceptibility measurements and the poor reproducibility of results have cast doubt on the bulk superconductivity in $La_3Ni_2O_7$ [7,11,15,19]. It is essential to examine the nature of the superconductivity in the bilayer nickelate $La_3Ni_2O_7$ and how this superconductivity evolves up to higher pressures.

In this work, we address these issues by conducting a detailed investigation of the high-pressure structural, electrical, and magnetic properties of $La_3Ni_2O_7$. Using neon gas as a pressure-transmitting medium, we observe a structural transition from orthorhombic to tetragonal symmetry above 40 GPa. High-pressure transport measurements reveal a SC phase diagram with a maximum T_c^{onset} of 83 K, which is suppressed above 80 GPa. Direct-current (DC) magnetic susceptibility measurements reveal the Meissner effect and confirm the bulk nature of superconductivity, with a SC volume fraction of ~41% at 22.0 GPa. These findings provide new insights into the relationship between superconductivity, oxygen content, and structural transitions in $La_3Ni_2O_7$.

RESULTS

High-pressure synchrotron XRD measurements were performed at the BL15U1 beamline of the Shanghai Synchrotron Radiation Facility (SSRF) using a wavelength of λ = 0.6199 Å. Polycrystalline samples of $La_3Ni_2O_7$ synthesized by the sol-gel method were used for these XRD measurements [15]. Single crystals of $La_3Ni_2O_7$ from the same batch, as we investigated before, were used for diamond anvil cell (DAC) electrical transport and DC magnetic susceptibility measurements [7,14,22]. Both polycrystalline and single-crystal samples were confirmed to exhibit the bilayer RP phase structure (see Fig. S1). A custom-designed miniature DAC made of beryllium-copper alloy was employed for ultrasensitive DC magnetic susceptibility measurements, which were conducted using a magnetic property measurement system (MPMS, Quantum Design, UK). The identical setup has successfully measured the Meissner effect in $La_4Ni_3O_{10}$ under pressure [23–26].

Our previous synchrotron XRD results indicated a structural transition from the *Amam* to the *Fmmm* space group at ~14 GPa when silicon oil was used as the pressure-transmitting medium (PTM) [7]. However, the pressure inhomogeneity induced by the solidification of silicon oil at 3 GPa and its glass-to-glass transitions at 10 and 16 GPa may have involved artifacts in the data analysis [27]. To mitigate these effects, we used neon gas as the PTM in the current high-pressure XRD study. An anomaly in the relative change of diffraction peaks was observed at 12.3 GPa (see Fig. S2), well above the crystallization pressure of 4.8 GPa and away from the non-hydrostatic pressure limit of 16.0 GPa for neon [28]. Figure 1b shows the pressure dependence of the peak widths of the (115) and (020)/(200)

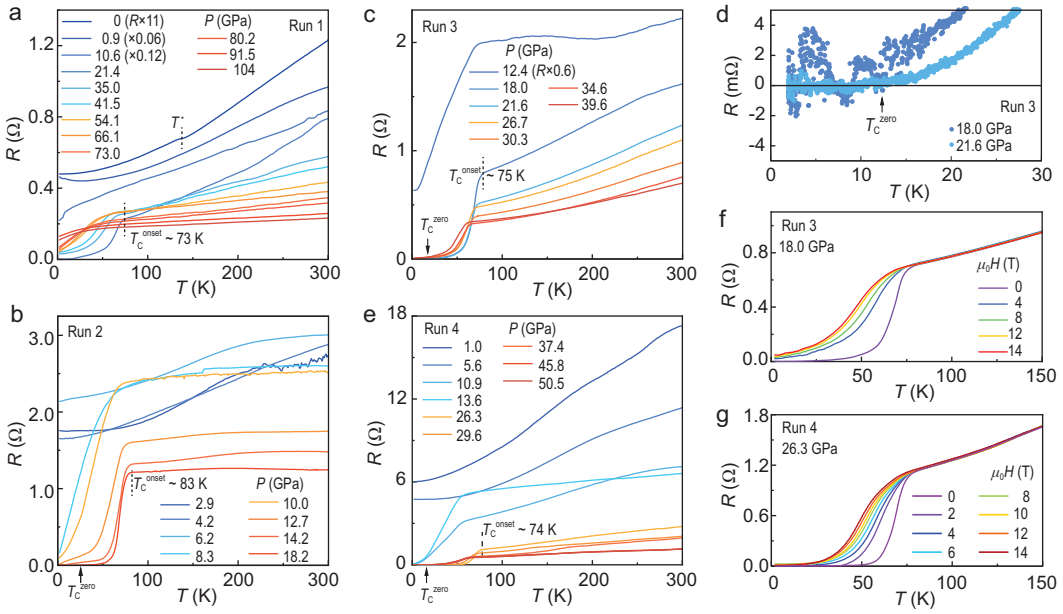

Figure 2. Temperature dependence of the in-plane resistance of $La_3Ni_2O_7$ under various pressures. (a–c, e) High-pressure resistance curves from run 1 to run 4. The resistance of $La_3Ni_2O_7$ from ambient pressure to 104 GPa is measured in run 1. A $T_c^{onset} \sim 83$ K is observed in run 2. (d) A zoom-in view of the resistance curves of run 3 under 18.0 and 21.6 GPa below 30 K. Zero resistance is achieved. (f, g) Field-dependent resistance curves at 18.0 GPa of run 3 and 26.3 GPa of run 4.

reflections. The peak widths broaden gradually with increasing pressure. The width of the (020)/(200) peak is broader than that of the (115) peak at low pressures due to the orthorhombicity, while they merge above 46.8 GPa, revealing a transition to a tetragonal structure (space group *I4/mmm*). A kink in the peak width of (020)/(200) at 12.3 GPa suggests a transition from the *Amam* to the *Fmmm* space group, as we proposed previously [7]. The refined lattice parameters are plotted in Fig. 1c and 1d.

The superconductivity in $La_3Ni_2O_7$ emerged from either a weakly insulating state or a metallic state at ambient pressure [7–11]. To ensure the reliability of our results, we performed high-pressure electrical transport measurements on five samples with similar dimensions ($30 \times 30 \times 10\ \mu m^3$) from the same batch. KBr was used as the PTM in these measurements. Figure 2a shows the resistance as a function of temperature at pressures ranging from 0 to 104 GPa. At ambient pressure, the resistance exhibits metallic behavior with an anomaly at $T^* \sim 140$ K, likely associated with a density-wave transition [14,26,29–32]. Under 0.9 GPa in run 1, the anomaly in resistance cannot be observed. A drop in resistance indicative of superconductivity is observed at 8 K and 10.6 GPa. The maximum T_c^{onset} of 73 K is achieved at 21.4 GPa in run 1, with a residual resistance of 1 mΩ at 2 K. Superconductivity is gradually suppressed and vanishes above 80.2 GPa. Figures 2b–2e and S3 show the high-pressure transport measurements on the other samples. The maximum T_c^{onset} reaches 83 K at 18.2 GPa in run 2, with zero resistance observed in runs 2, 3, and 4 (Fig. 2d), indicating high sample quality. The suppression of superconductivity by an external magnetic field is shown in Fig. 2f and 2g. A Ginzberg-Landau fitting yields an upper critical field of 126 T for run 4.

To further investigate the nature of the superconductivity in $La_3Ni_2O_7$ under pressure, we performed high-pressure DC magnetic susceptibility measurements to detect the Meissner effect. The DAC used in this experiment featured a pair of diamond anvils, each with a diameter of 400 μm. Non-magnetic rhenium gaskets were adopted to minimize the interference of the magnetic measurements. In run 1 of the DC susceptibility measurements, a single crystal of $La_3Ni_2O_7$ with dimensions of ~180 μm in diameter and 20 μm in thickness was placed in the sample chamber. Helium gas was used as the PTM to ensure optimal hydrostatic conditions. Distinct from the nearly constant background signals in Fig. 3a, significant diamagnetic behavior was observed around $T_c^{onset} \sim 76$ K under 22.0 GPa in both zero-field cooling (ZFC) and field cooling (FC) measurements in run 1 (Fig. 3b). The SC volume fraction was estimated to be 14% and 12% at 67 K for the ZFC and FC measurements, respectively. At lower temperatures, where the background susceptibility is unknown, the FC data were treated as the background and subtracted from the ZFC data to determine the SC

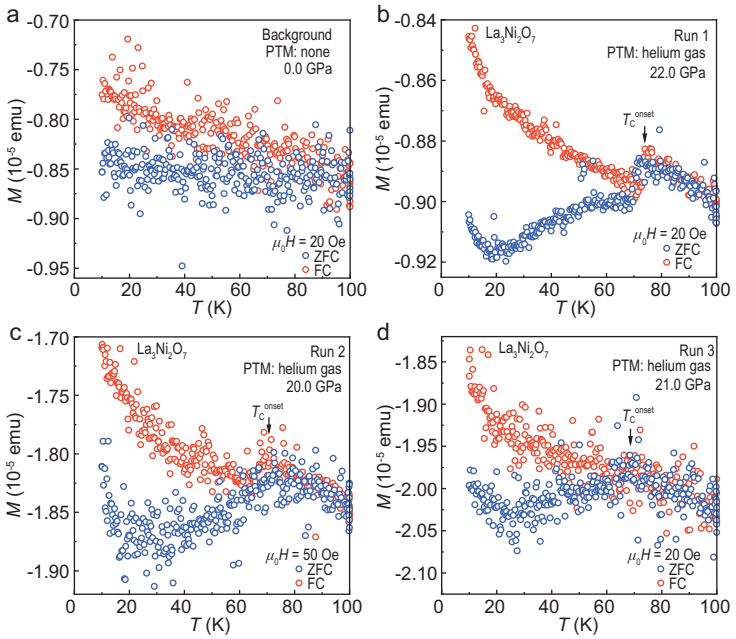

Figure 3. Direct-current magnetic susceptibility measurements of $La_3Ni_2O_7$ under pressure. Zero-field cooling (ZFC) and field cooling (FC) curves are measured with a field perpendicular to the *ab* plane. (a) Background signals of the high-pressure cell without a sample at ambient pressure. (b–d) Evident Meissner effect induced diamagnetic signals of pressurized $La_3Ni_2O_7$ single crystals from run 1 to run 3. Both ZFC and FC curves show prominent diamagnetic responses. The black arrows indicate the onset temperatures of superconductivity.

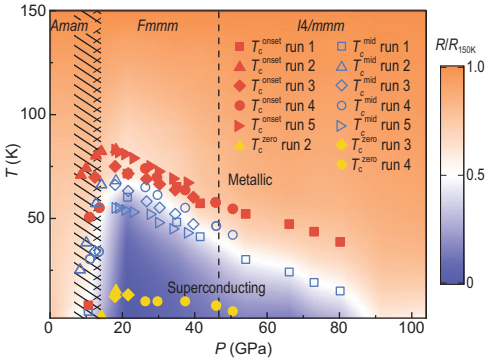

Figure 4. The superconducting phase diagram of $La_3Ni_2O_7$ single crystals under ambient pressure to 104 GPa. The red solid symbols represent the onset temperatures of superconductivity T_c^{onset} obtained from five runs. The blue hollow symbols represent the middle temperatures T_c^{mid} of the superconducting transition defined by the temperature corresponding to the resistance of $R_{mid} = (R_{onset} + R_{2K})/2$. The yellow dots mark the zero resistance temperatures T_c^{zero} of run 2 to run 4. The color of the ground shows the data of run 1. Structural transition pressures are indicated by the black striped lines and the dashed line.

volume fraction. This procedure yielded 41%, 31%, and 33% for runs 1, 2, and 3, respectively, as illustrated in Fig. 3b–3d. We note that the choice of background will lead to an underestimation of the SC volume fraction. Further details on the estimation method are provided in the Supplementary material. These results prove the Meissner effect and confirm the bulk superconductivity in $La_3Ni_2O_7$ single crystals.

DISCUSSION

The phase diagram and structural transitions of $La_3Ni_2O_7$ under high pressure are summarized in Fig. 4. The onset transition temperature T_c^{onset} is defined as the temperature at which the resistance drops, while the T_c^{mid} is the temperature at which the resistance is in the middle between that at the T_c^{onset} and 2 K. The background color scale represents the relative resistance change normalized to the value at 150 K in run 1. Superconductivity emerges as roughly coincidental with the structural transition from *Amam* to *Fmmm*, likely due to Fermi surface reconstruction or enhanced interlayer magnetic exchange coupling [33–44]. The T_c^{onset} reaches a maximum of 83 K at 18.0 GPa and decreases with increasing pressure, forming a right-triangle-like SC region. The T_c^{onset} drops to 38 K at 80.2 GPa, indicating a robust bulk SC phase in $La_3Ni_2O_7$. The orthorhombic structure revealed by XRD between 12.3 and 46.8 GPa suggests a tetragonal structure is not essential for the pressure-induced superconductivity in $La_3Ni_2O_7$.

The emergence of superconductivity in $La_3Ni_2O_7$ under high pressure is highly dependent on sample quality and pressure homogeneity [7–9,11]. Compared to La_2NiO_4 and $La_4Ni_3O_{10}$, the bilayer $La_3Ni_2O_7$ is a metastable phase with a narrower oxygen pressure window of 10–18 bar during the single crystal growth [45]. This complicates the sample synthesis, and sample inhomogeneity is hard to avoid. The other intergrowth phases, such as La_2NiO_4, $La_4Ni_3O_{10}$, and some other stacking sequences, are also possible [18,21,46]. While zero resistance and the Meissner effect have been observed in high quality single crystals, zero resistance is only achieved in small samples with a typical size of $30 \times 30 \times 10\ \mu m^3$ in our measurements. The SC volume fraction varies from a few percent in previous studies to ~41% in this work, likely due to variation in oxygen vacancy. STEM measurements have revealed that oxygen vacancies, particularly at the inner apical oxygen site, play a crucial role in suppressing superconductivity [13]. The inner apical oxygen is directly involved in the superexchange magnetic interactions between nickel ions along the *c*-axis and affects the splitting of the bonding and antibonding states of the $3d_{z^2}$ orbitals [7,39,47–50]. According to theoretical analysis, interlayer coupling

plays an important role in the superconductivity of pressurized $La_3Ni_2O_7$ [33,34,36,42–44,51–54]. Inelastic neutron scattering [55] and resonance inelastic X-ray scattering measurements [31] indeed reveal a strong interlayer coupling in $La_3Ni_2O_7$ compared to the dominant intralayer couplings in copper-based [56] and iron-based superconductors [57]. It is reasonable to argue that the inner apical oxygen vacancies will suppress superconductivity in the bilayer nickelate under pressure.

CONCLUSION

In conclusion, we have conducted a comprehensive study of the structural and SC properties of $La_3Ni_2O_7$ under high pressure. Our results reveal a structural transition from orthorhombic to tetragonal symmetry above 46.8 GPa and a right-triangle-like SC phase diagram with a maximum T_c^{onset} of 83 K. The SC phase is suppressed above 80 GPa, and DC magnetic susceptibility measurements reveal the Meissner effect and confirm the bulk nature of superconductivity with a SC volume fraction of ∼41% at 22.0 GPa and 20 K. These findings provide new insights into the relationship between superconductivity, oxygen content, and structural transitions in $La_3Ni_2O_7$, paving the way for further exploration of high-temperature superconductivity in nickelates.

SUPPLEMENTARY DATA

Supplementary data are available at *NSR* online.

ACKNOWLEDGMENTS

We thank the BL15U1 station and User Experiment Assist System of the Shanghai Synchrotron Radiation Facility (SSRF) for help in high-pressure structural characterizations.

FUNDING

Work at Sun Yat-sen University was supported by the National Natural Science Foundation of China (12425404, 12494591, 12474137, 12174454 and 12304187), the National Key Research and Development Program of China (2023YFA1406000 and 2023YFA1406500), the Guangdong Basic and Applied Basic Research Foundation (2024B1515020040 and 2024A1515030030), the Guangzhou Basic and Applied Basic Research Funds (2024A04J6417 and 2024A04J4024), the Shenzhen Science and Technology Program (RCYX20231211090245050), the Guangdong Provincial Key Laboratory of Magnetoelectric Physics and Devices (2022B1212010008), and the Research Center for Magnetoelectric Physics of Guangdong Province (2024B0303390001). D.P., Q.Z. and H.M. received support from the Shanghai Key Laboratory of Material Frontiers Research in Extreme Environments, China (22dz2260800), and the Shanghai Science and Technology Committee, China (22JC1410300).

AUTHOR CONTRIBUTIONS

M.W. designed the project. J.L., H.Z., H.D. and H.S. performed the high-pressure electricity and structural measurements. P.M., X.H., C.H., M.H., D.H., Z.D., X.C. and T.X. synthesized and characterized the samples at ambient pressure. D.P., Z.X., Q.Z. and H.M. conducted the high-pressure susceptibility measurements. M.W., J.L, P.D., H.S. and Q.Z. wrote the manuscript with inputs from all coauthors.

Conflict of interest statement. None declared.

REFERENCES

1. Božović I, Logvenov G, Butko V. Atomic-layer engineering of nickelates (in search of novel superconductors). *Physica C* 2023; **615**: 1354388.
2. Anisimov VI, Bukhvalov D, Rice TM. Electronic structure of possible nickelate analogs to the cuprates. *Phys Rev B* 1999; **59**: 7901–6.
3. Li D, Lee K, Wang BY *et al.* Superconductivity in an infinite-layer nickelate. *Nature* 2019; **572**: 624–7.
4. Zeng S, Tang CS, Yin X *et al.* Phase diagram and superconducting dome of infinite-layer $Nd_{1-x}Sr_xNiO_2$ thin films. *Phys Rev Lett* 2020; **125**: 147003.
5. Osada M, Wang BY, Goodge BH *et al.* A superconducting praseodymium nickelate with infinite layer structure. *Nano Lett* 2020; **20**: 5735–40.
6. Botana AS and Norman MR. Similarities and differences between $LaNiO_2$ and $CaCuO_2$ and implications for superconductivity. *Phys Rev X* 2020; **10**: 011024.
7. Sun H, Huo M, Hu X *et al.* Signatures of superconductivity near 80 K in a nickelate under high pressure. *Nature* 2023; **621**: 493–8.
8. Zhang Y, Su D, Huang Y *et al.* High-temperature superconductivity with zero resistance and strange-metal behaviour in $La_3Ni_2O_{7-\delta}$. *Nat Phys* 2024; **20**: 1269–73.
9. Hou J, Yang P-T, Liu Z-Y *et al.* Emergence of high-temperature superconducting phase in pressurized $La_3Ni_2O_7$ crystals. *Chin Phys Lett* 2023; **40**: 117302.
10. Zhang M, Pei C, Wang Q *et al.* Effects of pressure and doping on Ruddlesden-Popper phases $La_{n+1}Ni_nO_{3n+1}$. *J Mater Sci Technol* 2024; **185**: 147–54.
11. Zhou Y, Guo J, Cai S *et al.* Investigations of key issues on the reproducibility of high-T_c superconductivity emerging from compressed $La_3Ni_2O_7$. *Matter Radiat Extrem* 2025; **10**: 027801.
12. Sakakibara H, Ochi M, Nagata H *et al.* Theoretical analysis on the possibility of superconductivity in the trilayer uddlesden-popper nickelate $La_4Ni_3O_{10}$ under pressure and its experimental examination: comparison with $La_3Ni_2O_7$. *Phys Rev B* 2024; **109**: 144511.
13. Dong Z, Huo M, Li J *et al.* Visualization of oxygen vacancies and self-doped ligand holes in $La_3Ni_2O_{7-\delta}$. *Nature* 2024; **630**: 847–52.
14. Liu Z, Sun H, Huo M *et al.* Evidence for charge and spin density waves in single crystals of $La_3Ni_2O_7$ and $La_3Ni_2O_6$. *Sci China-Phys Mech Astron* 2022; **66**: 217411.

15. Wang G, Wang NN, Shen XL *et al.* Pressure-induced superconductivity in polycrystalline $La_3Ni_2O_7$. *Phys Rev X* 2024; **14**: 011040.
16. Wang N, Wang G, Shen X *et al.* Bulk high-temperature superconductivity in pressurized tetragonal $La_2PrNi_2O_7$. *Nature* 2024; **634**: 579–84.
17. Wang L, Li Y, Xie S-Y *et al.* Structure responsible for the superconducting state in $La_3Ni_2O_7$ at high-pressure and low-temperature conditions. *J Am Chem Soc* 2024; **146**: 7506–14.
18. Chen X, Zhang J, Thind AS *et al.* Polymorphism in the Ruddlesden–Popper nickelate $La_3Ni_2O_7$: discovery of a hidden phase with distinctive layer stacking. *J Am Chem Soc* 2024; **146**: 3640–5.
19. Puphal P, Reiss P, Enderlein N *et al.* Unconventional crystal structure of the high-pressure superconductor $La_3Ni_2O_7$. *Phys Rev Lett* 2024; **133**: 146002.
20. Abadi S, Xu K-J, Lomeli EG *et al.* Electronic structure of the alternating monolayer-trilayer phase of $La_3Ni_2O_7$. *Phys Rev Lett* 2025; **134**: 126001.
21. Wang H, Chen L, Rutherford A *et al.* Long-range structural order in a hidden phase of Ruddlesden–Popper bilayer nickelate $La_3Ni_2O_7$. *Inorg Chem* 2024; **63**: 5020–6.
22. Zhao D, Zhou Y, Huo M *et al.* Pressure-enhanced spin-density-wave transition in double-layer nickelate $La_3Ni_2O_{7-\delta}$. *Sci Bull* 2025; **70**: 1239–45.
23. Zhu Y, Peng D, Zhang E *et al.* Superconductivity in pressurized trilayer $La_4Ni_3O_{10-\delta}$ single crystals. *Nature* 2024; **631**: 531–6.
24. Li Q, Zhang Y-J, Xiang Z-N *et al.* Signature of superconductivity in pressurized $La_4Ni_3O_{10}$. *Chin Phys Lett* 2024; **41**: 017401.
25. Zhang M, Pei C, Peng D *et al.* Superconductivity in trilayer nickelate $La_4Ni_3O_{10}$ under pressure. *Phys Rev X* 2025; **15**: 021005.
26. Li J, Chen C-Q, Huang C *et al.* Structural transition, electric transport, and electronic structures in the compressed trilayer nickelate $La_4Ni_3O_{10}$. *Sci China-Phys Mech Astron* 2024; **67**: 117403.
27. Chen X, Lou H, Zeng Z *et al.* Structural transitions of 4:1 methanol–ethanol mixture and silicone oil under high pressure. *Matter Radiat Extrem* 2021;**6**: 038402.
28. Klotz S, Chervin JC, Munsch P *et al.* Hydrostatic limits of 11 pressure transmitting media. *J Phys D Appl Phys* 2009; **42**: 075413.
29. Wu G, Neumeier JJ, Hundley MF. Magnetic susceptibility, heat capacity, and pressure dependence of the electrical resistivity of $La_3Ni_2O_7$ and $La_4Ni_3O_{10}$. *Phys Rev B* 2001; **63**: 245120.
30. Liu Z, Huo M, Li J *et al.* Electronic correlations and partial gap in the bilayer nickelate $La_3Ni_2O_7$. *Nat Commun* 2024; **15**: 7570.
31. Chen X, Choi J, Jiang Z *et al.* Electronic and magnetic excitations in $La_3Ni_2O_7$. *Nat Commun* 2024; **15**: 9597.
32. Chen K, Liu X, Jiao J *et al.* Evidence of spin density waves in $La_3Ni_2O_{7-\delta}$. *Phys Rev Lett* 2024; **132**: 256503.
33. Yang Y-f, Zhang G-M, Zhang F-C. Interlayer valence bonds and two-component theory for high-*Tc* superconductivity of $La_3Ni_2O_7$ under pressure. *Phys Rev B* 2023; **108**: L201108.
34. Lu C, Pan Z, Yang F *et al.* Interlayer-coupling-driven high-temperature superconductivity in $La_3Ni_2O_7$ under pressure. *Phys Rev Lett* 2024; **132**: 146002.
35. Sakakibara H, Kitamine N, Ochi M *et al.* Possible high *Tc* superconductivity in $La_3Ni_2O_7$ under high pressure through manifestation of a nearly half-filled bilayer hubbard model. *Phys Rev Lett* 2024; **132**: 106002.
36. Luo Z, Hu X, Wang M *et al.* Bilayer two-orbital model of $La_3Ni_2O_7$ under pressure. *Phys Rev Lett* 2023; **131**: 126001.
37. Christiansson V, Petocchi F, Werner P. Correlated electronic structure of $La_3Ni_2O_7$ under pressure. *Phys Rev Lett* 2023; **131**: 206501.
38. Zhang Y, Lin L-F, Moreo A *et al.* Structural phase transition, $s_{\pm}$-wave pairing, and magnetic stripe order in bilayered superconductor $La_3Ni_2O_7$ under pressure. *Phys Rev Lett* 2024; **15**: 2470.
39. Wang Y, Jiang K, Wang Z *et al.* Electronic and magnetic structures of bilayer $La_3Ni_2O_7$ at ambient pressure. *Phys Rev B* 2024; **110**: 205122.
40. Wú W, Luo Z, Yao D-X *et al.* Superexchange and charge transfer in the nickelate superconductor $La_3Ni_2O_7$ under pressure. *Sci China-Phys Mech Astron* 2024; **67**: 117402.
41. Fan Z, Zhang J-F, Zhan B *et al.* Superconductivity in nickelate and cuprate superconductors with strong bilayer coupling. *Phys Rev B* 2024; **110**: 024514.
42. Oh H and Zhang Y-H. Type-ii *t-j* model and shared superexchange coupling from Hund's rule in superconducting $La_3Ni_2O_7$. *Phys Rev B* 2023; **108**: 174511.
43. Yang H, Oh H, Zhang Y-H. Strong pairing from a small Fermi surface beyond weak coupling: application to $La_3Ni_2O_7$. *Phys Rev B* 2024; **110**: 104517.
44. Ryee S, Witt N, Wehling TO. Quenched pair breaking by interlayer correlations as a key to superconductivity in $La_3Ni_2O_7$. *Phys Rev B* 2024; **133**: 096002.
45. Zhang J, Zheng H, Chen Y-S *et al.* High oxygen pressure floating zone growth and crystal structure of the metallic nickelates $R_4Ni_3O_{10}$ (R = La, Pr). *Phys Rev Mater* 2020;**4**: 083402.
46. Li F, Guo N, Zheng Q *et al.* Design and synthesis of three-dimensional hybrid Ruddlesden-Popper nickelate single crystals. *Phys Rev Mater* 2024;**8**: 053401.
47. Geisler B, Fanfarillo L, Hamlin JJ *et al.* Optical properties and electronic correlations in $La_3Ni_2O_7$ bilayer nickelates under high pressure. *npj Quantum Mater* 2024;**9**: 89.
48. Liu Y-B, Mei J-W, Ye F *et al.* $s^{\pm}$-Wave pairing and the destructive role of apical-oxygen deficiencies in $La_3Ni_2O_7$ under pressure. *Phys Rev Lett* 2023; **131**: 236002.
49. Yi X-W, Meng Y, Li J-W *et al.* Nature of charge density waves and metal-insulator transition in pressurized $La_3Ni_2O_7$. *Phys Rev B* 2024; **110**: L140508.
50. Yang J, Sun H, Hu X *et al.* Orbital-dependent electron correlation in double-layer nickelate $La_3Ni_2O_7$. *Nat Commun* 2024; **15**: 4373.
51. Yang Q-G, Wang D, Wang Q-H. Possible s±-wave superconductivity in $La_3Ni_2O_7$. *Phys Rev B* 2023; **108**: L140505.
52. Kaneko T, Sakakibara H, Ochi M *et al.* Pair correlations in the two-orbital Hubbard ladder: implications for superconductivity in the bilayer nickelate $La_3Ni_2O_7$. *Phys Rev B* 2024; **109**: 045154.
53. Luo Z, Lv B, Wang M *et al.* High-T_c superconductivity in $La_3Ni_2O_7$ based on the bilayer two-orbital t-J model. *npj Quantum Mater* 2024;**9**: 61.
54. Zheng Y-Y and Wú W. $s_{\pm}$-Wave superconductivity in the bilayer two-orbital Hubbard model. *Phys Rev B* 2025; **111**: 035108.
55. Xie T, Huo M, Ni X *et al.* Strong interlayer magnetic exchange coupling in $La_3Ni_2O_{7-\delta}$ revealed by inelastic neutron scattering. *Sci Bull* 2024; **69**: 3221–7.
56. Headings NS, Hayden SM, Coldea R *et al.* Anomalous high-energy spin excitations in the high-*Tc* superconductor-parent antiferromagnet La_2CuO_4. *Phys Rev Lett* 2010; **105**: 247001.
57. Dai P. Antiferromagnetic order and spin dynamics in iron-based superconductors. *Phys Rev Lett* 2015; **87**: 855–96.